Available online at BCREC website: https://bcrec.id

Bulletin of Chemical Reaction Engineering & Catalysis, 17 (4) 2022, 850-861

Research Article

Synthesis of p-Aminophenol from p-Nitrophenol Using CuO-Nanoleaf/γ-Al_2O_3 Catalyst

Didik Sudarsono[1,2], Eriawan Rismana[2], S. Slamet[1,*]

[1]Department of Chemical Engineering, Universitas Indonesia, Depok, 16425, Indonesia.
[2]Research Center for Pharmaceutical Ingredients and Traditional Medicine, National Research and Innovation Agency, Jakarta, 10340, Indonesia.

Received: 11th October 2022; Revised: 16th December 2022; Accepted: 19th December 2022
Available online: 21st December 2022; Published regularly: December 2022

Abstract

The CuO-nanoleaf/γ-Al_2O_3 catalyst was synthesized through wet chemical impregnation and had promising catalytic activity in reducing p-Nitrophenol (PNP) into p-Aminophenol (PAP). The synthesis was conducted in situ with Ethylene Glycol as a stabilizer agent of the CuO-nanoleaf structure and γ-Al_2O_3 as catalyst support with high adsorption ability. Furthermore, the crystal phase, morphology, element composition, and specific surface area were investigated by X-Ray Diffraction (XRD), Field Emission Scanning Electron Microscopy (FESEM), and N_2 adsorption-desorption, respectively. The XRD pattern showed the crystal phase of CuO and γ-Al_2O_3 in the composite, and the morphology was successfully reported using FESEM. The increase in the specific surface area of the catalyst indicates that the CuO material was well composited in γ-Al_2O_3. The catalyst has good activity in reducing PNP to PAP with 93.53% PNP conversion within 4 min. In addition, the reduction reaction of PNP with excess $NaBH_4$ could be categorized as pseudo-first order kinetic with a constant rate of 0.4852 min^{-1} for CuO-nanoleaf/γ-Al_2O_3 catalyst. The loading catalyst and temperature reaction effect on PNP conversion were also investigated. The results showed that 94.18% PNP conversion was obtained within only 2.5 min under the optimized conditions.

Keywords: p-Aminophenol; p-Nitrophenol; CuO; γ-Al_2O_3; Nanoleaf

How to Cite: D. Sudarsono, E. Rismana, S. Slamet (2022). Synthesis of p-Aminophenol from p-Nitrophenol Using CuO-Nanoleaf/γ-Al_2O_3 Catalyst. *Bulletin of Chemical Reaction Engineering & Catalysis*, 17(4), 850-861 (doi: 10.9767/bcrec.17.4.16135.850-861)

Permalink/DOI: https://doi.org/10.9767/bcrec.17.4.16135.850-861

1. Introduction

p-Aminophenol (PAP) is widely used as a colouring agent, fragrance agent, corrosion inhibitor, resin manufacturer, and medicinal raw materials in the pharmaceutical industry [1–3]. PAP is non-toxic and an essential intermediate compound in the manufacture of antipyretic and analgesic drugs such as Paracetamol [4]. This drug is widely used to reduce headaches, minor aches, and fevers. The need for Paracetamol is relatively high, reaching 8,000 tons/year in Indonesia, hence, PAP synthesis technology is necessary. The formation of PAP can be conducted with catalytic conversion of p-Nitrophenol (PNP) in the presence of $NaBH_4$ [5,6]. According to several types of research, noble metal catalysts, including Pd, Pt, Ag, and Au, can be used in the reduction process of PNP to PAP [7–14]. However, PNP reduction requires high costs and tends to agglomerations after use [15]. Catalytic transformation using metal oxide catalysts such as CuO is an alternative method for synthesizing PAP due to its advantageous physicochemical characteristics [16–18].

* Corresponding Author.
Email: slamet@che.ui.ac.id (S. Slamet);
Telp: +62-21-7863516, Fax: +62-21-7863515

Morphology and size can influence the physicochemical properties of nano-material. Therefore, the performance of the CuO can be improved by changing its morphology to form nanosheets, nanorods, nanowires, nanoflowers, or other nanostructures. Che *et al.* [19] examined how morphology of CuO nanostructures affected the catalytic activity to transform PNP to PAP. The reaction rate constant for the CuO-nanoleaf structure was more excellent than CuO nanoflower and nano-dumbbell structures. According to Bhattacharjee *et al.* [20], the CuO nanorods structure had a more excellent reaction rate constant than the nanosheet structure. Sahu *et al.* [21] researched the use of CuO nanowire catalyst to reduce PNF into PAP, where the catalytic activity provided was high with a reaction rate constant of 0.5014 min^{-1}.

Several methods of preparation of CuO nanostructures have been developed, such as hydrothermal [22,23], microwave-assist [24], thermal decomposition [25], electrodeposition [26], and wet chemical route [18,27,28]. The wet chemical method is an alternative for preparing CuO nanostructures because its a more direct process and a lower production cost than other methods [29]. The limitation is low adsorption capacity, which tends to agglomerations within a specific time and catalysts accumulate to large aggregates and micron-sized entities [19]. It reduces the active site and specific surface area for the desired reaction. The combination of CuO nanostructure with γ-Al_2O_3 can increase the adsorption ability of composite and reduce the agglomeration process of catalyst [30]. The γ-Al_2O_3 has a crystal structure with a high specific surface area, pore volume, and an open type of mesoporosity that allows rapid penetration into the active site of the catalyst [31,32].

A few research focused on using CuO nanostructure catalyst without support for applying PNP reduction. In this study, CuO-nanoleaf structure was impregnated with γ-Al_2O_3 for reduction of PNP to PAP. This was formed through a supported catalyst with the wet chemical impregnation method. Adding γ-Al_2O_3 improves adsorption capacity with a high specific surface area and reduces agglomeration. The CuO-nanoleaf/γ-Al_2O_3 catalyst was characterized by Field Emission Scanning Electron Microscopy-Energy Dispersive Spectroscopy (FESEM-EDS), X-Ray Diffraction (XRD), and Brunauer, Emmett, and Teller (BET). In particular, the effects of adding γ-Al_2O_3, loading catalyst, temperature reaction, and their catalytic performance in terms of PNP reduction into PAP were emphasized.

2. Materials and Methods

2.1 Materials

Copper Sulfate Pentahydrate (Merck, 99%), Sodium Hydroxide (Merck, 99%), Ethylene Glycol (Merck, 99,5%), and γ-Al_2O_3 (Merck, 99%) with pro-analysis grade were used for the synthesis catalyst. In addition, p-Nitrophenol (Merck, 99,5%) and $NaBH_4$ (Merck, 98%) with pro-analysis grade were applied to analyze the catalytic performance and produce p-Aminophenol.

2.2 Synthesis CuO-nanoleaf/γ-Al_2O_3

The CuO-nanoleaf/γ-Al_2O_3 catalyst was prepared by using the wet chemical method. Initially, 100 mL of 0.125 M $CuSO_4.5H_2O$ solution was made in demin water, and 10 mL of Ethylene Glycol (EG) with and without 20 g of γ-Al_2O_3 were added to the solution while stirring with 500 rpm for 30 min. During the mixing process, 50 mL of 0.6 M sodium hydroxide was added dropwise to the solution. Subsequently, the solution was mixed at 90 °C and stirred continuously for 2 h. The precipitate formed was centrifuged, washed with water and ethanol until pH 7. It was dried in a vacuum oven for 12 h at 60 °C, and the resultant powder was ground, sieved with a 100 mesh sieve, and calcined in an atmospheric furnace at 350 °C within 4 h.

2.3 Characterization

The dry samples were analyzed for physical properties such as crystal phase, specific surface area, pore volume, morphology, and element composition. XRD with the brand Shimadzu X-Ray Diffractometer XD-610 was utilized to evaluate the crystal phase of materials with Cu anode (Kα 1.5406 Å) as beam source, operation under 30 mA and 40 kV, with the 2θ range of 20–80. N_2 adsorption–desorption isotherms were obtained using Micromeritics Tristar 3020 surface area and a porosimetry analyzer instrument at liquid nitrogen temperature 77 K with the brand Quantachrome Nova 4200e. The specific surface area was calculated using the Brunauer-Emmett-Teller (BET) equation. The morphology and element composition of nanoleaf CuO catalysts were analyzed using FESEM-EDS with the brand JEOL JIB-4610F employing the accelerating voltage of 15 kV.

The catalytic properties of decreasing PNP concentration to produce PAP were analyzed using a UV-VIS spectrophotometer with the brand Libra S70PC. The loading of copper (Cu) in the catalyst was determined by Inductively Coupled Plasma (ICP).

2.4 Catalytic Performance

In reactor glass, PAP was produced from PNP with the presence of a CuO-nanoleaf/γ-Al_2O_3 catalyst. Before the tests, several solutions were newly made, and 100 mL of 2.2×10^{-4} M PNP and 1.58×10^{-2} M $NaBH_4$ solution were prepared. In a typical process, PNP and $NaBH_4$ solution were mixed in reactor glass, and 150 mg of the CuO-nanoleaf/γ-Al_2O_3 catalyst was added under stirring. Furthermore, the solution kept the reaction temperature at 30 °C, and a UV-visible spectrophotometer was used to examine the absorbance spectrum. The change in the PNP peak intensity after 2 ml aliquots were periodically obtained, filtered, and measured. For the catalyst reusability test, the spent catalyst was filtered from the solution and dried at a temperature of 90 °C. After that, the spent catalyst was reused for PNP reduction under a similar condition operation in several consecutive runs.

3. Results and Discussion

3.1 Morphology

Figures 1(a) and (b) show FESEM images from the CuO-nanoleaf and CuO-nanoleaf/γ-Al_2O_3 catalyst with 50K magnification, respectively. Based on Figure 1(a), CuO-nanoleaf was synthesized by the method used and was accumulated between catalysts. The Nanoleaf CuO structures had a thickness, wideness, and length range of 20 to 40 nm, 50 nm, and 200 nm. Based on Figure 1(b), CuO with nanoleaf structures was attached to the surface of γ-Al_2O_3. Therefore, adding γ-Al_2O_3 does not affect the formation of CuO-nanoleaf structure using the wet chemical method. On

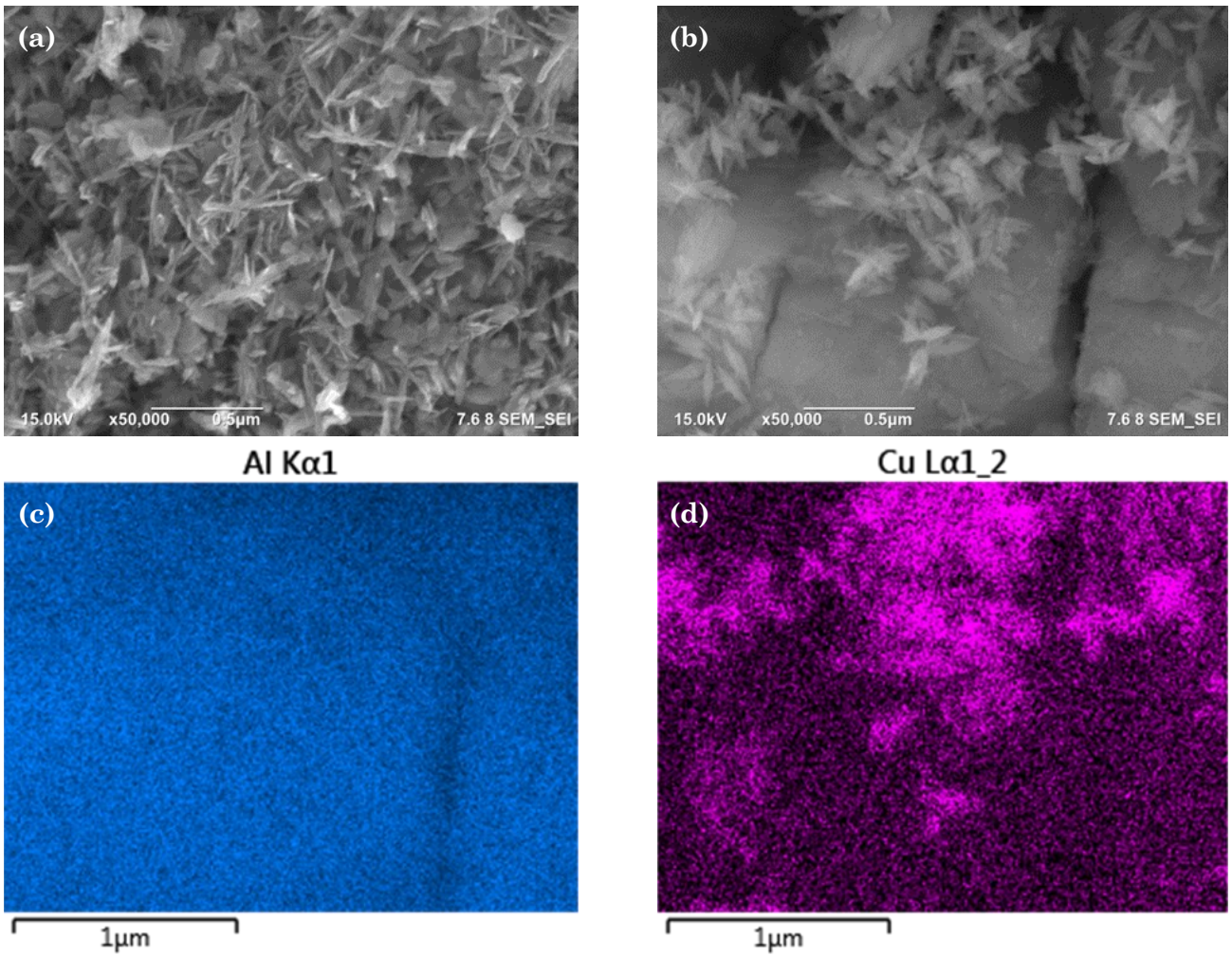

Figure 1. FESEM image of (a) synthesized CuO-nanoleaf and (b) CuO-nanoleaf/γ-Al_2O_3 catalyst, element mapping of (c) Al Kα1, and (d) Cu Lα1_2 in CuO-nanoleaf/γ-Al_2O_3 catalyst.

the surface of γ-Al_2O_3, the nanoleaf CuO structures were distributed equally and covered most of the γ-Al_2O_3 surface. The nanoleaf CuO structures were obtained due to the addition of Ethylene Glycol as a stabilizer agent, with a reaction temperature of 363 K within 2 h [17]. On the other hand, γ-Al_2O_3 used had a cubic shape particle with a solid rough structure with a side range of 20 μm.

The CuO-nanoleaf's distribution on the surface of γ-Al_2O_3 was analyzed through EDS mapping. The element mapping of Al Kα1 (Figure 1(c)) and Cu Lα1 (Figure 1(d)) was measured in synthesized CuO-nanoleaf/γ-Al_2O_3. Therefore, the nanoleaf structure was a CuO catalyst while the cubic shape below the was γ-Al_2O_3 support. Figure 2 shows the EDS spectra of the synthesized CuO-nanoleaf/γ-Al_2O_3 catalyst with 1000x magnification. The composition of Cu, Al, and O element without other elements indicates a proper manufacturing process, and the purification can remove several contaminants, according to washing with water and ethanol. Figure 2 shows the EDS spectra of the synthesized CuO-Nanoleaf/γ-Al_2O_3 catalyst with 1000x magnification. The EDS analysis of CuO-nanoleaf/γ-Al_2O_3 catalyst confirmed the Cu content of 5.12 %wt. In addition, the Cu content in the CuO-nanoleaf/γ-Al_2O_3 catalyst also measures with the ICP method. The ICP result showed the Cu content in the CuO-nanoleaf/γ-Al_2O_3 catalyst was about 3.75 %.

3.2 Crystal Structure

The XRD pattern of the synthesized catalyst prepared by similar experimental conditions is shown in Figure 3. The XRD pattern of CuO-nanoleaf (without γ-Al_2O_3) with the peak at 2θ

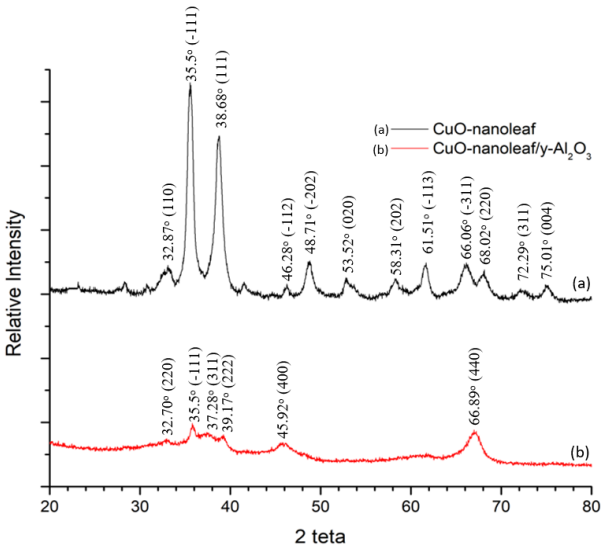

Figure 3. XRD pattern of CuO-nanoleaf and CuO-nanoleaf/γ-Al_2O_3 catalyst.

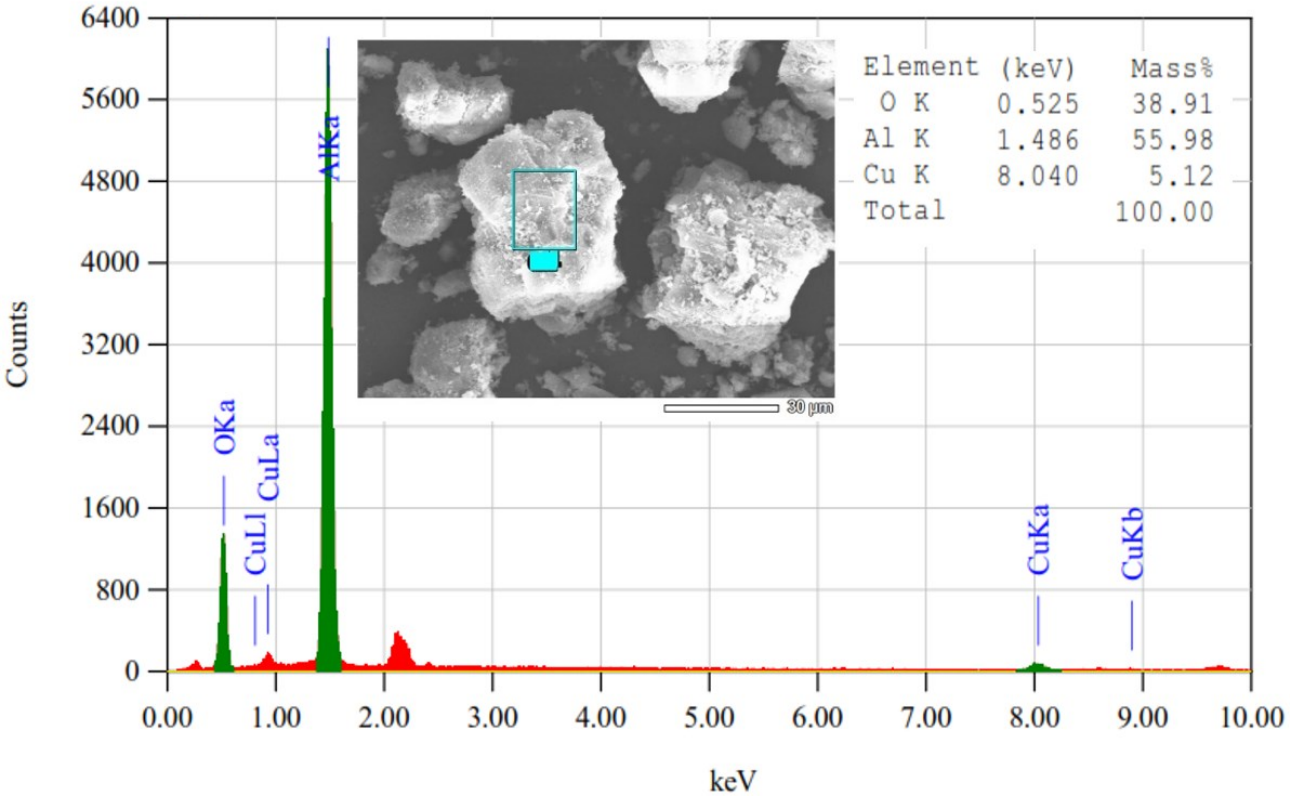

Figure 2. EDS spectra of synthesized CuO-nanoleaf/γ-Al_2O_3 catalyst.

values of 32.87°, 35.54°, 38.68°, 46.28°, 48.71°, 53.52°, 58.31°, 61.51°, 66.06°, 68.02°, 72.29°, and 75.01° were associated with the (110), (−111), (111), (−112), (−202), (020), (202), (−113), (−311), (220), (311), and (004) reflections plane, respectively. Meanwhile, the diffraction peaks can be indexed in the monoclinic CuO phase with the JCPDS (Joint Committee on Powder Diffraction Standard) card files no. 89-5895 [21,33]. The lattice parameters were calculated using the Rietveld refinement analysis from the Reitica program. The Rietveld method fits the experimental data to the calculated data profile (structure crystal CuO with monoclinic crystalline with an instrumental parameter, such as vector $a \neq b \neq c$ and angle $\alpha = \gamma = 90° \neq \beta$). The obtained parameters were a = 4.6893 Å, b = 3.4268 Å, c = 5.1321 Å, $\alpha = \gamma = 90.00$ and $\beta = 99.653°$ with volume cell of 81.27 Å^3. The result indicated that the synthesized CuO was monoclinic crystalline, unlike the tenorite phase, which shaped a tri-clinic lattice with unequal unit cell length of a = 3.74 Å, b = c = 4.67 Å. Impurity peaks, such as $Cu(OH)_2$, Cu_2O, Cu, or precursors, were not detected, indicating that the product was relatively pure.

The XRD pattern of CuO-nanoleaf/γ-Al_2O_3 catalysts showed diffraction peaks at 2θ of 32.70°, 37.28°, 39.17°, 45.92°, and 66.89°, representing (220), (311), (222), (400), and (440) at crystal planes of the γ-Al_2O_3, respectively [34]. No clear diffraction peaks of crystalline CuO were visible in the CuO-nanoleaf/γ-Al_2O_3 catalysts XRD pattern. This shows that γ-Al_2O_3 was a dominantly crystal phase and a small portion of crystalline CuO that dispersity on the surface of γ-Al_2O_3. The XRD confirmed the EDS spectrum result where the quantity of γ-Al_2O_3 in the CuO-nanoleaf/γ-Al_2O_3 composite was very dominating, as evidenced by the peak of the Al element being higher than the Cu element. The research conducted by Nandanwar *et al.* [35] and Hua *et al.* [36] showed the same condition, with no apparent peaks of crystalline CuO appearing in the XRD pattern of the synthesized CuO-nanoparticle/Al_2O_3 composite.

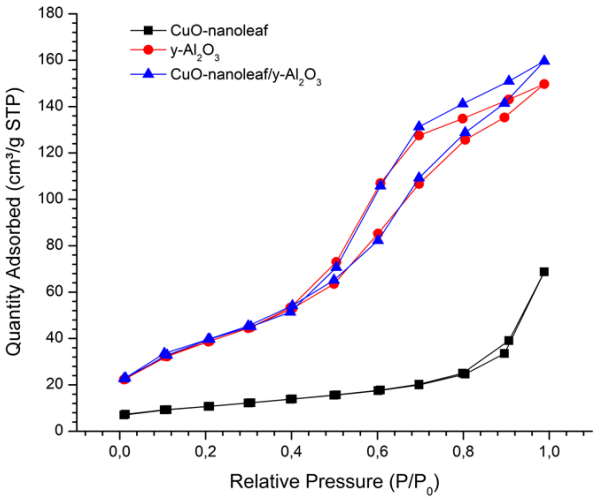

Figure 4. N_2 adsorption-desorption isotherm of CuO-nanoleaf, γ-Al_2O_3, and CuO-nanoleaf/γ-Al_2O_3.

3.3 Specific Surface Area

The N_2 adsorption-desorption profile of CuO-nanoleaf, γ-Al_2O_3, and CuO-nanoleaf/γ-Al_2O_3 catalysts is given in Figure 4. Furthermore, the observed isotherms were classified as type IV with a composite pore size of 7.04 nm. This is consistent with the mesoporous catalytic support with pore sizes between 2 and 50 nm [34]. Multi-point BET equation was used to calculate the specific surface areas of catalysts. Table 1 shows the results of BET surface area and average pore volume of CuO-nanoleaf, γ-Al_2O_3, and CuO-nanoleaf/γ-Al_2O_3 catalysts derived from nitrogen physisorption. The results of BET surface area of CuO-nanoleaf, γ-Al_2O_3, and CuO-nanoleaf/γ-Al_2O_3 catalyst was 37.53 $m^2.g^{-1}$, 137.32 $m^2.g^{-1}$, and 140.19 $m^2.g^{-1}$, respectively.

The synthesized CuO-nanoleaf catalyst had a relatively low BET surface area, and γ-Al_2O_3 material had a high adsorption capacity with a high surface area. The BET surface area increased significantly when CuO-nanoleaf was loaded on the γ-Al_2O_3 surface from 37.53 $m^2.g^{-1}$ to 140.19 $m^2.g^{-1}$, which could increase the adsorption capacity of the CuO-nanoleaf/γ-Al_2O_3 composite. The composite had a slightly higher value of BET surface area than γ-Al_2O_3 material. This is because the EDS spectrum confirmed only a small addition of CuO to the composite. Pan *et al.* [32] and Antony *et al.* [34] showed that the addition of CuO nanoparticles catalyst to the Al_2O_3 in the composite gave a higher value of BET surface area. The CuO-nanoleaf, γ-Al_2O_3, and CuO-nanoleaf/γ-Al_2O_3 catalyst had an average pore volume of 0.106 $cm^3.g^{-1}$, 0.231 $cm^3.g^{-1}$, and 0.247 $cm^3.g^{-1}$, respectively.

Table 1. Surface properties of CuO-nanoleaf, γ-Al_2O_3, and CuO-nanoleaf/γ-Al_2O_3 catalyst.

Sample	S_{BET} ($m^2.g^{-1}$)	V_{pore} ($cm^3.g^{-1}$)
CuO	37.53	0.106
γ-Al_2O_3	137.32	0.231
CuO/γ-Al_2O_3	140.19	0.247

3.4 Catalytic Performance

PAP was synthesized with reduction of the PNP method with excess $NaBH_4$ in an aqueous solution to investigate the catalytic activities of the CuO-nanoleaf/γ-Al_2O_3 composite. UV-visible spectroscopy was used to evaluate the reduction reaction of PNP. Meanwhile, when $NaBH_4$ is added to the PNP solution, the colour changes from light to intense yellow. Only an absorption peak at 400 nm was seen in the spectrum, indicating the formation of 4-nitrophenolate anions as an intermediate [18,37,38]. The stability of the intermediate may be shown by the absence of a drop in the absorption peak at 400 nm in the absence of a catalyst [19,39]. Figure 5 shows the UV–visible absorption spectrum of PNP solution with various reaction times in the presence of CuO-nanoleaf/γ-Al_2O_3 catalyst. The peak intensity of 400 nm significantly decreased when the CuO-nanoleaf/γ-Al_2O_3 catalyst was added to the PNP solution. In contrast, a new adsorption peak appeared at 233 nm and 300 nm in the UV-visible spectrum, indicating the formation of PAP in the solution [40]. UV-visible spectra showed that PNP and by-products were undetectable at the end of the reaction solution. Therefore, PNP reacts with $NaBH_4$ to produce the required products when CuO-nanoleaf/γ-Al_2O_3 catalysts are added.

CuO-nanoleaf, γ-Al_2O_3, and CuO-nanoleaf/γ-Al_2O_3 catalysts were used to reduce PNP to PAP and create various catalytic performances.

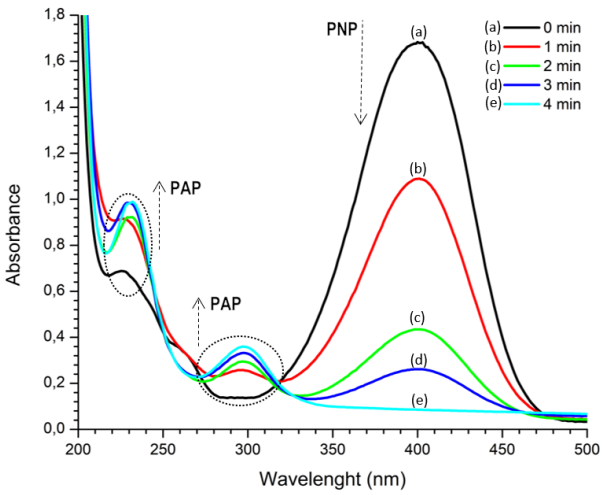

Figure 5. The UV–visible absorption spectrum of the systems containing PNP and $NaBH_4$ in the presence of CuO-nanoleaf/γ-Al_2O_3 (PNP initial concentration = 2.2×10^{-4} M, $NaBH_4$ initial concentration = 1.58×10^{-2} M, loading catalyst = 150 mg and reaction temperature = 30 °C).

As illustrated in Figure 6, it takes longer than 20 min for a 15 mg CuO-nanoleaf catalyst to convert PNP to PAP. After using 150 mg of the CuO-nanoleaf/γ-Al_2O_3 catalyst (prediction 15 mg active site CuO in composite), it only took 4 min to reduce PNP to PAP. Using a 150 mg CuO-nanoleaf catalyst, the conversion of PNP to PAP took 5 minutes. The production of PAP did not occur with the used γ-Al_2O_3 catalyst without the active site of CuO, indicated by the absence of a peak at 300 nm. Meanwhile, γ-Al_2O_3 was inactive as a catalyst for converting the PNP reduction process to PAP. The decrease in peak intensity at 400 nm was due to the adsorption process of PNP on the pore of the γ-Al_2O_3 catalyst. The absence of any catalyst in the solution indicated a slight increase in PNP conversion until 1% in the PNP hydrogenation reaction. It demonstrates that the CuO-nanoleaf or CuO-nanoleaf/γ-Al_2O_3 catalyst was an important substance in the PNP reduction reaction. On the other hand, the experiment with the absence of $NaBH_4$ in the solution had also been done, and the result indicated no change in the PNP conversion (<0.5%). $NaBH_4$ substance was a critical compound in producing hydrogen gas which was used as a reactant for the PNP reduction reaction. $NaBH_4$ generated H_2, and the active site of CuO-nanoleaf/γ-Al_2O_3 catalyst were important substances in the PNP reduction reaction to produce PAP compound.

The initial concentration of $NaBH_4$ was very high compared to the initial PNP

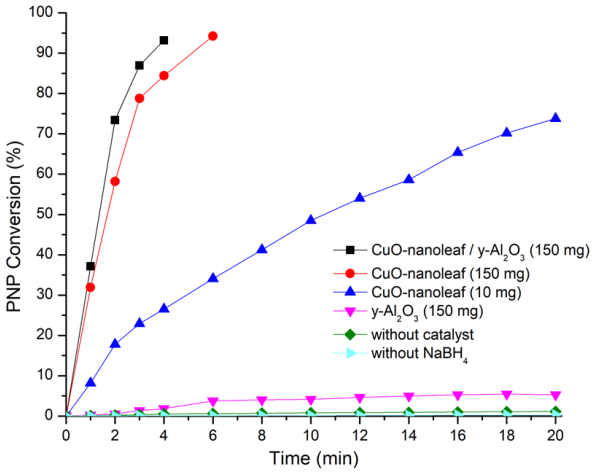

Figure 6. The PNP conversion vs reaction time curves in the presences of 150 mg CuO-nanoleaf/γ-Al_2O_3, 150 mg CuO-nanoleaf, 10 mg CuO-nanoleaf, 150 mg γ-Al_2O_3, catalyst, and without catalyst, respectively (PNP initial concentration = 2.2×10^{-4} M, $NaBH_4$ initial concentration = 1.58×10^{-2} M, temperature reaction 30 °C).

concentration. Therefore, the concentration was still constant during the PNP reduction. The reaction of PNP to PAP could be regarded as pseudo first order kinetic with excess $NaBH_4$ [18,19], as represented in Equation (1). In this equation, C_0, C, k, and t represent the initial concentration of PNP, instantaneous concentrations of PNP, pseudo-first-order rate constant, and reaction time, respectively. The pseudo-first-order rate constant (k) was determined from the linear plots' slopes by fitting lines using the raw data between $\ln(C_0/C)$ and response time.

$$\ln\left(\frac{C_0}{C}\right) = kt \quad (1)$$

Table 2 shows the constant rate value of CuO-nanoleaf, CuO-nanoleaf/γ-Al_2O_3, and γ-Al_2O_3 catalysts with various loading catalysts. The constant rate was calculated at a low PNP conversion (below 20%) in the early reaction. PNP conversions for the CuO-nanoleaf and CuO-nanoleaf/γ-Al_2O_3 catalysts with loading catalyst 150 mg were calculated with time intervals of 20 s until 60 s. On the other hand, PNP conversions for the CuO-nanoleaf catalyst with loading catalyst 150 mg was calculated with time intervals of 1 min until 3 min.

The rate constants were calculated to be 0.4852 min^{-1} for CuO-nanoleaf/γ-Al_2O_3, 0.4336 min^{-1} for CuO-nanoleaf, and 0.0039 min^{-1} for γ-Al_2O_3 with loading catalyst 150 mg in solution. The rate constant using CuO-nanoleaf/γ-Al_2O_3 catalyst was slightly higher than CuO-nanoleaf catalyst under the same opera-ting conditions. The catalytic process for reducing PNP depends on the presence of active site CuO and the addition of γ-Al_2O_3 to the composite. The rate constant in PNP reduction using CuO nanoleaf/γ-Al_2O_3 catalyst 150 mg was higher than CuO-nanoleaf catalyst 10 mg without γ-Al_2O_3 (EDS prediction with 10 mg active site CuO in composite) with rate constant of 0.0898 min^{-1} under the same reduction condition. The reaction rate constant of nanoleaf/γ-Al_2O_3 catalyst was 5.40 times greater than CuO nanoleaf catalyst without γ-Al_2O_3 material. In the experiment, the catalyst was prepared by grinding and sieving with a 100-mesh sieve. In addition, the PNP reduction reaction stirring was carried out at a rotational speed of 500 rpm. The tiny size of the catalyst and the fast rotational speed of the reaction affect the surface reaction of the catalyst as a limiting reaction rather than external diffusion.

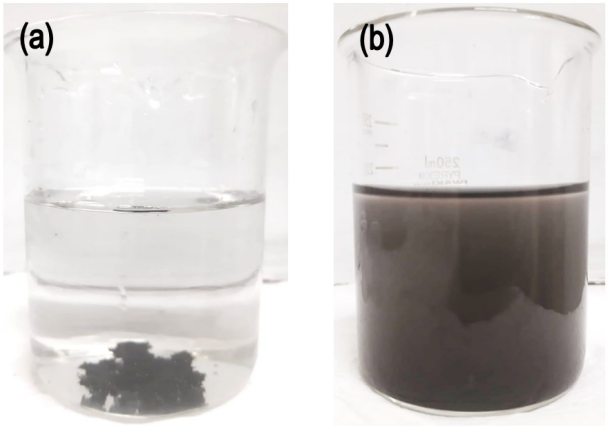

Figure 7. Visual condition after PNP reduction using (a) CuO-nanoleaf, and (b) CuO-nanoleaf/γ-Al_2O_3, catalyst.

The experiment observed the agglomeration process when CuO-nanoleaf catalyst was added to the reactor. This could significantly reduce the specific surface area of the catalyst, as shown in Figure 7(a). The CuO-nanoleaf/γ-Al_2O_3 catalyst showed different results where no agglomeration occurred, and the catalyst remained well distributed in the solution, as shown in Figure 7(b). The FESEM image showed that the γ-Al_2O_3 could reduce the agglomeration process by dispersing CuO-nanoleaf on the surface of γ-Al_2O_3 and also increase the specific surface area of the catalyst, confirmed with the BET. The large specific surface area of CuO-nanoleaf/γ-Al_2O_3 catalyst could efficiently increase the adsorption ability to adsorb 4-nitrophenolate anions. γ-Al_2O_3 support was acidic material where phenol compound could be adsorbed on both acidic and basic catalysts [41]. Therefore, using CuO-nanoleaf impregnated with γ-Al_2O_3 could increase the catalytic activity and be higher than using CuO-nanoleaf catalyst without support. On the other hand, the CuO-

Table 2. Rate constant value of CuO-nanoleaf, γ-Al_2O_3, and CuO-nanoleaf/γ-Al_2O_3 catalyst.

Catalyst	Loading catalyst (mg)	Rate Constant (10^{-2} min^{-1})	Correlation Coefficient, R^2
CuO-nanoleaf/γ-Al_2O_3	150	48.52	0.9988
CuO-nanoleaf	150	43.36	0.9993
CuO-nanoleaf	10	8.98	0.9968
γ-Al_2O_3	150	0.72	0.9788

nanoleaf/γ-Al_2O_3 catalyst can be recovered by using a filtration process to separate the catalyst from the reaction solution.

The possible mechanism of catalytic heterogeneity for PAP production using CuO-nanoleaf/γ-Al_2O_3 catalyst was described in Figure 8. Initially, $NaBH_4$ reacts with two moles of water to become one mole of $NaBO_2$ and four moles of hydrogen gas. This gas was adsorbed on the catalyst surface with dissociative adsorption, establishing the required H^* to reduce PNP [16,42]. In addition, the 4-Nitrophenolate ions as a reactant were adsorbed on the surface of the CuO-nanoleaf/γ-Al_2O_3 catalyst. The surface reaction between 4-nitrophenolate ions and H^* then becomes PAP on the surface of the CuO-nanoleaf/γ-Al_2O_3 catalyst. Finally, the desorption process of PAP occurs when PAP release from the surface of the CuO-nanoleaf/γ-Al_2O_3 catalyst. γ-Al_2O_3 material could increase the adsorption ability to adsorb the 4-nitrophenolate ions and H^* in solution to reach the surface of CuO-nanoleaf, hence, the reaction mechanism occurs faster. On the other hand, the BH_4^- ions are also adsorbed to the surface of the CuO-nanoleaf/γ-Al_2O_3 catalyst and transfer electrons to the 4-nitrophenolate ions for the PNP reduction process to become PAP product [43].

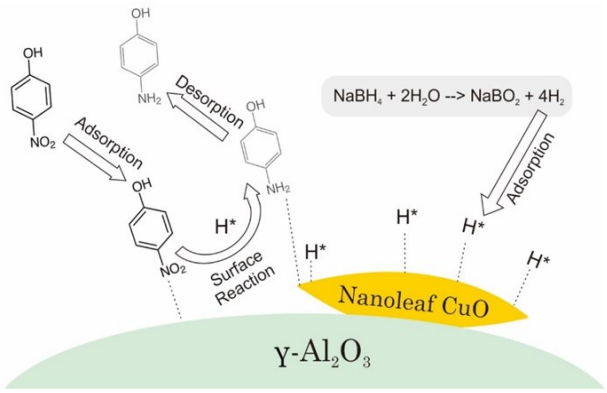

Figure 8. Mechanism reaction of PNP conversion to PAP using CuO-nanoleaf/γ-Al_2O_3.

Generally, a catalyst's ability to catalyze reactions can be affected by the number of active sites on the composite. Figure 9(a) shows that PNP conversion increased with the increasing catalyst loading. The higher the catalyst loading, the greater the active site of the catalyst, and the higher the catalytic activity ability is for PNP reduction. PNP conversion significantly increased when adding catalyst loading was 75 to 150 mg. PNP conversion was obtained to be 40.16% and 93.53%, with catalyst loading of 75 mg and 150 mg, respectively, with a reaction time of 4 minutes and keeping other conditions constant. Figure 9(b) shows the constant rate values vs catalyst loading. The rate constant in 75 mg of catalyst loading was obtained to be 21.6×10^{-2} min^{-1}. A further increase in catalyst loading increased the rate constant linearly, which means the catalytic activity would increase. The research by Nandawar *et al.* [35] showed the same results where the rate constant increased with increasing loading catalyst using CuO-nanoparticle/Al_2O_3 catalyst. A further rise in catalyst loading does not increase PNP conversion when adding catalyst loading from 150 mg to 200 mg. At this stage, increasing the number of active sites of CuO does not affect raising the reaction constant for reducing PNP. The greater the concentration of the catalyst in the solution, the more likely it is to cover the

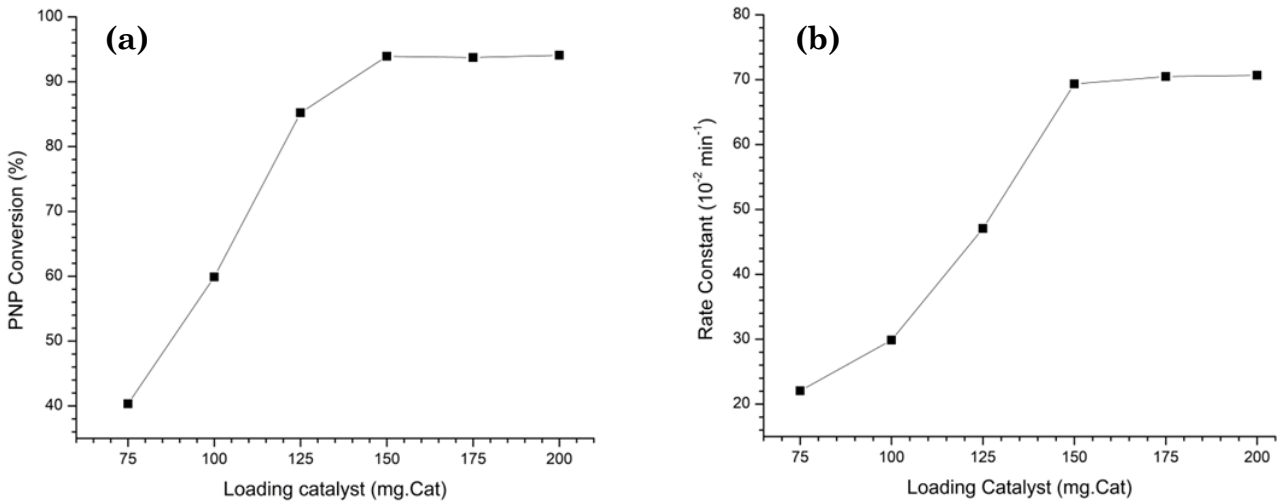

Figure 9. (a) PNP conversion vs loading catalyst curve and (b) Rate constant vs loading catalyst curve with CuO-nanoleaf/γ-Al_2O_3 catalyst on PNP reduction (PNP initial concentration = 2.2×10^{-4} M, $NaBH_4$ initial concentration = 1.58×10^{-2} M, reaction temperature 30 °C, reaction time 4 min).

catalyst's active site, which has no influence on the performance.

The reduction process also depends on the reaction temperature, which was altered from 20 to 50 °C while maintaining the same reduction conditions. Figure 10 shows that PNP conversion increase with the temperature reaction. In 2.5 min, the PNP conversion could reach 72.43% at a smaller reaction temperature of 20 °C and 94.18% at 50 °C. The higher the reaction temperature, the greater the rate constant obtained, and the greater the PNP reduction catalytic activity capability. The activation energy was found to be 20.57 kJ.mol^{-1} (Figure 10 inserted) from kinetic data and calculated with the Arrhenius equation. Nandanwar *et al.* (2012) found that the activation energy was 27.41 kJ/mol using colloidal CuO/Al_2O_3 as a catalyst for PNP reduction reaction [35].

3.5 Catalyst Reusability Test

Reusability is one of the important virtues of the catalyst. The reusability of the as-prepared CuO-nanoleaf/γ-Al_2O_3 catalyst in the PNP reduction process were further investigated. After the catalyst was used in a catalytic reduction process, the catalyst was separated from the solution by filtration of the solution followed by washing it with water and dry the catalyst. Then, the CuO-nanoleaf/γ-Al_2O_3 catalyst was again used as a catalyst in another run of PNP reduction reaction. Figure 11 shows the PNP conversion vs a number of cycles of catalyst usage. The CuO-nanoleaf/γ-Al_2O_3 catalyst had been used four times for catalyzing the same reaction. The PNP conversion value still remain more than 80% after the catalyst was reused in four times. It shows their reusability and stability for the CuO-nanoleaf/γ-Al_2O_3 catalyst for PNP reduction process while keeping its high catalytic activity. To evaluate the reason, the Cu content in spent catalyst after removing the catalyst from the reaction was analyzed by ICP. The result show that there was no obvious leaching of copper during the reaction with Cu content of catalyst after reusability test was 3.41%.

4. Conclusion

In summary, the CuO-nanoleaf/γ-Al_2O_3 catalyst was synthesized by a wet chemical impregnation method. The results showed that CuO with nanoleaf structure was attached and distributed on the surface of γ-Al_2O_3, increasing the specific surface area of the catalyst and decreasing a tendency to agglomeration. The CuO-nanoleaf/γ-Al_2O_3 catalyst was used to produce PAP by reducing PNP in the presence of $NaBH_4$ and has high catalytic activity with a constants rate of 0.4862 min^{-1} and 93.53 % PNP conversion within 4 min. The catalyst loading and temperature reaction parameters greatly affected the synthesis of PAP from the reduction of PNP. The optimum parameters were a catalyst loading of 150 mg, a temperature reaction of 50 °C with a PNP initial concentration of 2.2×10^{-4} M, and $NaBH_4$ of 1.58×10^{-2} M. The results showed that 94.18% PNP conversion was obtained within

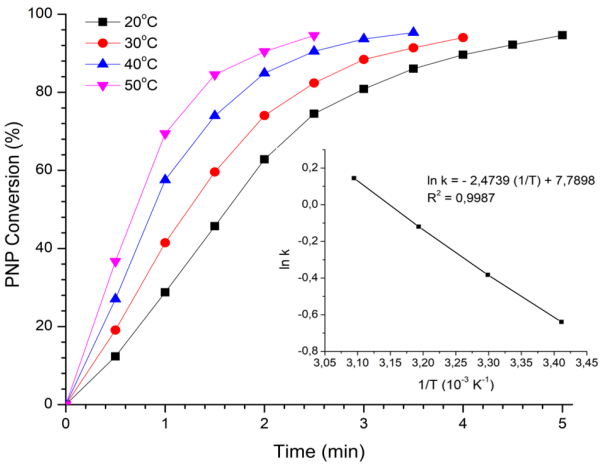

Figure 10. PNP conversion vs time reaction curve and ln k vs $1/T$ curve with nanoleaf CuO/γ-Al_2O_3 catalyst on PNP reduction (PNP initial concentration = 2.2×10^{-4} M, $NaBH_4$ initial concentration = 1.58×10^{-2} M, loading catalyst = 150 mg).

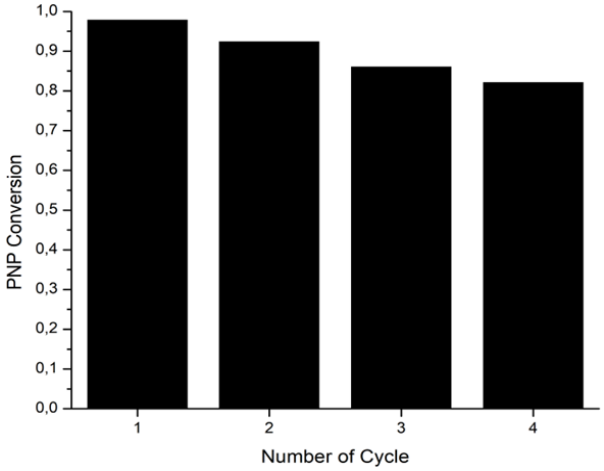

Figure 11. PNP Conversion vs number of cycles in multiple cycles using CuO-nanoleaf/γ-Al_2O_3 catalyst (PNP initial concentration = 2.2×10^{-4} M, $NaBH_4$ initial concentration = 1.58×10^{-2} M, loading catalyst = 150 mg, reaction temperature 30 °C, time reaction 10 min).

2.5 min under the optimized condition. The CuO-nanoleaf/γ-Al_2O_3 catalyst can promise practical application in the synthesis of PAP. This is because of its high catalytic efficiency and low cost in the synthesis process.

Acknowledgments

The authors would like to acknowledge the financial support of the Saintek scholarship / BRIN Scholarship from the National Research and Innovation Agency for financially supporting this research. We also thank the Research Center for Pharmaceutical Ingredients and Traditional Medicine, National Research and Innovation Agency South Tangerang, Banten, for providing facilities for this research.

CRediT Author Statement

Author Contributions: D. Sudarsono: Conceptualization, Methodology, Investigation, Resources, Data Curation, Writing, Draft Preparation, Review and Editing, Project Administration; E. Rismana: Validation, Writing, Review and Editing, Data Curation; Slamet : Conceptualization, Methodology, Formal Analysis, Data Curation, Writting, Supervision. All authors have read and agreed to the published version of the manuscript.

References

[1] Du, Y., Chen, H., Chen, R., Xu, N. (2004). Synthesis of p-aminophenol from p-nitrophenol over nano-sized nickel catalysts. *Applied Catalysis A: General,* 277 (1-2), 259-264. DOI: 10.1016/j.apcata.2004.09.018.

[2] Rode, C., Vaidya, M., Jaganathan, R., Chaudhari, R. (2001). Hydrogenation of nitrobenzene to p-aminophenol in a four-phase reactor: reaction kinetics and mass transfer effects. *Chemical Engineering Science,* 56 (4), 1299-1304. DOI: 10.1016/S0009-2509(00)00352-3.

[3] Komatsu, T., Hirose, T. (2004). Gas phase synthesis of para-aminophenol from nitrobenzene on Pt/zeolite catalysts. *Applied Catalysis A: General,* 276 (1-2), 95-102. DOI: 10.1016/j.apcata.2004.07.044.

[4] Dai, M., Li, H.X., Lang, J.P. (2015). New approaches to the degradation of organic dyes, nitro- and chloro-aromatics using coordination polymers as photocatalysts. *CrystEngComm,* 17, 4741-4753. DOI: 10.1039/C5CE00619H.

[5] Swathi, T., Buvaneswari, G. (2008). Application of $NiCo_2O_4$ as a catalyst in the conversion of p-nitrophenol to p-aminophenol. *Materials Letters,* 62(23), 3900-3902. DOI: 10.1016/j.matlet.2008.05.028.

[6] Ellis, F. (2002). *Paracetamol: a curriculum resource*. Royal Society of Chemistry.

[7] Chang, Y.C., Chen, D.H. (2009). Catalytic reduction of 4-nitrophenol by magnetically recoverable Au nanocatalyst. *Journal of Hazardous Materials,* 165(1-3), 664-669. DOI: 10.1016/j.jhazmat.2008.10.034

[8] Lee, J.H., Hong, S.K., Ko, W.B. (2011). Reduction of 4-Nitrophenol Catalyzed by Platinum Nanoparticles Embedded into Carbon Nanocolloid. *Asian Journal of Chemistry,* 23(5), 2347-2350.

[9] Mohamed, M.M., Al-Sharif, M.S. (2012). One pot synthesis of silver nanoparticles supported on TiO_2 using hybrid polymers as template and its efficient catalysis for the reduction of 4-nitrophenol. *Materials Chemistry and Physics,* 136(2-3), 528-537. DOI: 10.1016/j.matchemphys.2012.07.021.

[10] Nemanashi, M., Meijboom, R. (2013). Synthesis and characterization of Cu, Ag and Au dendrimer-encapsulated nanoparticles and their application in the reduction of 4-nitrophenol to 4-aminophenol. *Journal of Colloid and Interface Science,* 389(1), 260-267. DOI: 10.1016/j.jcis.2012.09.012.

[11] Hernández-Gordillo, A., Arroyo, M., Zanella, R., Rodríguez-González, V. (2014). Photoconversion of 4-nitrophenol in the presence of hydrazine with AgNPs-TiO_2 nanoparticles prepared by the sol–gel method. *Journal of Hazardous Materials,* 268, 84-91. DOI: 10.1016/j.jhazmat.2013.12.069.

[12] Jiang, H., Yan, Q., Du, Y., Chen, R. (2016). Synthesis of p-aminophenol from p-nitrophenol reduction over Pd@ ZIF-8. *Reaction Kinetics, Mechanisms and Catalysis,* 117(1), 307-317. DOI: 10.1007/s11144-015-0928-y.

[13] Motta, D. Sanchez, F., Alshammari, K., Chincilla, L. E., Botton, G A., Morgan, D., Tabanelli, T., Villa, A., Hammond, C., Dimitratos, N. (2019). Preformed Au colloidal nanoparticles immobilised on NiO as highly efficient heterogeneous catalysts for reduction of 4-nitrophenol to 4-aminophenol. *Journal of Environmental Chemical Engineering,* 7(5), 103381. DOI: 10.1016/j.jece.2019.103381.

[14] Tian, X., Zahid, M., Li, J., Sun, W., Niu, X., Zhu, Y. (2020). Pd/Mo_2N-TiO_2 as efficient catalysts for promoted selective hydrogenation of 4-nitrophenol: A green bio-reducing preparation method. *Journal of Catalysis,* 391, 190-201. DOI: 10.1016/j.jcat.2020.08.027

[15] Wunder, S., Polzer, F., Lu, Y., Mei, Y., Ballauff, M. (2010). Kinetic analysis of catalytic reduction of 4-nitrophenol by metallic nanoparticles immobilized in spherical polyelectrolyte brushes. *The Journal of Physical Chemistry C,* 114(19), 8814-8820. DOI: 10.1021/jp101125j.

[16] Kassem, A. A., Abdelhamid, H. N., Fouad, D. M., Ibrahim, S. A. (2020). Catalytic reduction of 4-nitrophenol using copper terephthalate frameworks and CuO@ C composite. *Journal of Environmental Chemical Engineering,* 9(1), 104401. DOI: 10.1016/j.jece.2020.104401.

[17] Aditya, T., Jana, J., Singh, N., Pal, K. A., Pal, T. (2017). Remarkable Facet Selective Reduction of 4-Nitrophenol by Morphologically Tailored (111) Faceted Cu_2O Nanocatalyst. *ACS Omega,* 2(5), 1968-1984. DOI: 10.1021/acsomega.6b00447.

[18] Sahu, K., Singh, J., Mohapatra, S. (2019). Catalytic reduction of 4-nitrophenol and photocatalytic degradation of organic pollutants in water by copper oxide nanosheets. *Optical Materials,* 93, 58-69. DOI: 10.1016/j.optmat.2019.05.007.

[19] Che, W., Ni, Y., Zhang, Y., Ma, Y. (2015). Morphology-controllable synthesis of CuO nanostructures and their catalytic activity for the reduction of 4-nitrophenol. *Journal of Physics and Chemistry of Solids,* 77, 1-7. DOI: 10.1016/j.jpcs.2014.09.006.

[20] Bhattacharjee, A., Ahmaruzzaman, M. (2016). CuO nanostructures: facile synthesis and applications for enhanced photodegradation of organic compounds and reduction of p-nitrophenol from aqueous phase. *RSC Advances,* 6(47), 41348-41363. DOI: 10.1039/C6RA03624D.

[21] Sahu, K., Singhal, R., Mohapatra, S. (2020). Morphology controlled CuO nanostructures for efficient catalytic reduction of 4-nitrophenol. *Catalysis Letters,* 150(2), 471-481. DOI: 10.1007/s10562-019-03009-w.

[22] Anu Prathap, M.U., Kaur, B., Srivastava, R. (2012). Hydrothermal synthesis of CuO micro-/nanostructures and their applications in the oxidative degradation of methylene blue and non-enzymatic sensing of glucose/H_2O_2. *Journal of Colloid and Interface Science,* 370(1), 144-154. DOI: 10.1016/j.jcis.2011.12.074.

[23] Hong, J., Li, J., Ni, Y. (2009). Urchin-like CuO microspheres: Synthesis, characterization, and properties. *Journal of Alloys and Compounds,* 481(1-2), 610-615. DOI: 10.1016/j.jallcom.2009.03.043.

[24] Zhang, M., Xu, X., Zhang, M. (2008). Microwave-Assisted Synthesis and Characterization of CuO Nanocrystals. *Journal of Dispersion Science and Technology,* 29(4), 508-513. DOI: 10.1080/01932690701728734.

[25] Gao, D., Yang, G., Li, J., Zhang, J., Zhang, J., Xue, D. (2010). Room-temperature ferromagnetism of flowerlike CuO nanostructure. *The Journal of Physical Chemistry C,* 114(43), 18347-18351. DOI: 10.1021/jp106015t.

[26] Chen, L., Shet, S., Tang, H., Wang, H., Deutsch, T., Yan, Y., Turner, T., Al-Jassim, M. (2010). Electrochemical deposition of copper oxide nanowires for photoelectrochemical applications. *Journal of Materials Chemistry,* 20(33), 6962-6967. DOI: 10.1039/C0JM01228A.

[27] Ethiraj, A.S., Kang, D.J. (2012). Synthesis and characterization of CuO nanowires by a simple wet chemical method. *Nanoscale research letters,* 7(1), 70. DOI: 10.1186/1556-276X-7-70.

[28] Wang, W., Liu, Z., Liu, Y., Xu, C., Zheng, C., Wang, G. (2003). A simple wet-chemical synthesis and characterization of CuO nanorods. *Applied Physics A,* 76(3), 417-420. DOI: 10.1007/s00339-002-1514-5.

[29] Sahu, K., Satpati, B., Singhal, R., Mohapatra, S. (2020). Enhanced catalytic activity of CuO/Cu_2O hybrid nanowires for reduction of 4-nitrophenol in water. *Journal of Physics and Chemistry of Solids,* 136, 109143. DOI: 10.1016/j.jpcs.2019.109143.

[30] Farahmandjou, M., Golabiyan, N. (2019). Synthesis and characterisation of Al_2O_3 nanoparticles as catalyst prepared by polymer coprecipitation method. *Materials Engineering Research,* 1(2), 40-44. DOI: 10.25082/MER.2019.02.002.

[31] Ali, S., Abbas, Y., Zuhra, Z., Butler, I.S. (2019). Synthesis of γ-alumina (Al_2O_3) nanoparticles and their potential for use as an adsorbent in the removal of methylene blue dye from industrial wastewater. *Nanoscale Advances,* 1(1), 213-218. DOI: 10.1039/C8NA00014J.

[32] Pan, W., Zhang, G., Zheng, T., Wang, P. (2015). Degradation of p-nitrophenol using CuO/Al_2O_3 as a Fenton-like catalyst under microwave irradiation. *RSC Advances,* 5(34), 27043-27051. DOI: 10.1039/C4RA14516J.

[33] Kamal, T. (2019). Aminophenols formation from nitrophenols using agar biopolymer hydrogel supported CuO nanoparticles catalyst. *Polymer Testing,* 77, 105896. DOI: 10.1016/j.polymertesting.2019.105896.

[34] Antony, A., Sun, M.Y., Jin-Hyo, B., You, H.B. (2018). Nano sheets, needles and grains-like CuO/γ-Al_2O_3 catalysts' performance in carbon monoxide oxidation. *Journal of Solid State Chemistry,* 265, 431-439. DOI: 10.1016/j.jssc.2018.06.031.

[35] Nandanwar, S.U., Chakraborty M. (2012). Synthesis of colloidal CuO/γ-Al_2O_3 by micro-emulsion and its catalytic reduction of aromatic nitro compounds. *Chinese Journal of Catalysis,* 33(9-10), 1532-1541. DOI: 10.1016/S1872-2067(11)60433-6.

[36] Hua, L. Ma, H. Zhang, L. (2013). Degradation process analysis of the azo dyes by catalytic wet air oxidation with catalyst CuO/γ-Al_2O_3. *Chemosphere,* 90(2), 143-149. DOI: 10.1016/j.chemosphere.2012.06.018.

[37] Filiz, B.C. (2020). The role of catalyst support on activity of copper oxide nanoparticles for reduction of 4-nitrophenol. *Advanced Powder Technology,* 31(9), 3845-3859. DOI: 10.1016/j.apt.2020.07.026.

[38] Das, R., Sypu, V.S., Paumo, H.K., Bhaumik, M., Maharaj, V., Maity, A. (2019). Silver decorated magnetic nanocomposite (Fe_3O_4@PPy-MAA/Ag) as highly active catalyst towards reduction of 4-nitrophenol and toxic organic dyes. *Applied Catalysis B: Environmental,* 244, 546-558. DOI: 10.1016/j.apcatb.2018.11.073.

[39] Sharma, M., Hazra, S., Basu, S. (2017). Synthesis of heterogeneous Ag-Cu bimetallic monolith with different mass ratios and their performances for catalysis and antibacterial activity. *Advanced Powder Technology,* 28(11), 3085-3094. DOI: 10.1016/j.apt.2017.09.023.

[40] Du, X., He, J., Zhu, J., Sun, L., An, S. (2012). Ag-deposited silica-coated Fe_3O_4 magnetic nanoparticles catalyzed reduction of p-nitrophenol. *Applied Surface Science,* 258(7), 2717-2723. DOI: 10.1016/j.apsusc.2011.10.122.

[41] Tanabe, Y., Nishibayashi, Y. (2013). Developing more sustainable processes for ammonia synthesis. *Coordination Chemistry Reviews,* 257(17), 2551-2564. DOI: 10.1016/j.ccr.2013.02.010.

[42] Hashimi, A.S., Nohan, M.A.N.M., Chin, S.X., Zakaria, S. Chia, C.H. (2019). Rapid catalytic reduction of 4-nitrophenol and clock reaction of methylene blue using copper nanowires. *Nanomaterials,* 9(7), 936. DOI: 10.3390/nano9070936.

[43] Fu, L., Zhou, W., Wen, M., Wu, Q., Li, W., Wu, D., Zhu, Q., Ran, J., Ren, P. (2021). Layered CuNi-Cu_2O/$NiAlO_x$ nanocatalyst for rapid conversion of p-nitrophenol to p-aminophenol. *Nano Research,* 14(12), 4616-4624. DOI: 10.1007/s12274-021-3391-2.